The Effect of PWHT on Electrochemical Behaviour of AISI 316L Weld Metal

S. Kožuh,[a,*] M. Gojić,[a] and M. Kraljić Roković[b]
[a]Faculty of Metallurgy, University of Zagreb,
Aleja narodnih heroja 3, 44103 Sisak, Croatia
[b]Faculty of Chemical Engineering and Technology,
University of Zagreb, Savska cesta 16/I, 10000 Zagreb, Croatia

Original scientific paper
Received: January 30, 2008
Accepted: September 29, 2008

The subject of investigation was the corrosion behaviour of AISI 316L austenitic stainless steel weld metal as dependent on a protective passive film formed on the steel surface following exposure to w = 3.5 % NaCl. The corrosion properties were examined before PWHT and after it by means of cyclic polarization, electrochemical impedance spectroscopy, and chronoamperometric measurements. Cyclic polarization curves clearly indicated a decrease in the pitting potential following PWHT. Passivity was observed over a broad potential region. Charge transfer resistance associated with the corrosion resistance of the passive film as determined by electrochemical impedance spectroscopy indicated that high temperature PWHT acted by increasing the thickness of the passive film.

Key words:
Austenitic stainless steel, weld metal, microstructure, pitting corrosion, passive film

Introduction

Austenitic stainless steels find a wide range of applications in industry, mainly in aggressive environments, because of corrosion resistance and weldability. The corrosion resistance of these steels depends on various metallurgical variables such as grain size, alloy composition, previous deformation, solution annealing, post-weld heat treatment (PWHT), etc. Owing to a high amount of alloying elements, austenitic stainless steels tend to exhibit rather complex precipitation behaviour.[1,2] The precipitation of intermetallic phases and carbides induced by welding and PWHT can cause chromium depletion near the grain boundaries. This can lead to the phenomenon known as sensitization, when the depleted zones become the focus of intense corrosion.[3] To lower the sensitization level, the carbon content of the overlaid weld metal must be controlled carefully. The sensitization behaviour can also be influenced by the content of the ferrite phase and its distribution in the weld metal. Austenitic stainless steels may become sensitized to corrosion if they are exposed to a temperature between ϑ = 600 and 900 °C, or subjected to slow cooling. The pitting corrosion of the weld metal is of great practical interest. In engineering structures, it can prove to be a destructive form of corrosion as it may cause perforation of equipment.[4,5] Most equipment failures are due to pitting corrosion induced by chloride ions.

Passivation of metals and metallic alloys is of considerable technical importance.[6] The microstructural changes provoked by elevated temperatures in austenitic stainless steels may enhance susceptibility to corrosion. A breakdown of corrosion resistance is generally due to chromium depletion in the zones adjacent to the chromium-rich precipitates (i.e. sigma, chi or Z-phases). Devoid of chromium, these zones become susceptible to corrosion attack. Exposure to thermal treatment causes precipitation of sigma phase (Fe-Cr-Mo) or carbides ($Cr_{23}C_6$), which weakens the passivity of stainless steel and facilitates corrosion. Sigma phase is known mostly to exert a negative impact on the mechanical properties and corrosion resistance.[1–3]

With a passive film present, corrosion takes place through outward diffusion of cations and inward diffusion of anions. The film components should thus possess the ability to act as diffusion barriers. The stability of the passive film can vary. It will depend on alloy composition, operating environment, film thickness, its structure, stoichiometry, electronic band structure, ionic conductivity, etc. As a collective noun, stainless steels denote alloys that mainly consist of iron, chromium and nickel. The most important alloying element is chromium, which is responsible for the formation of a protective oxide film. According to the literature,[7] the alloy must contain at least 13 % chromium to form a stable passive film. In a study on Cr-Ni steels by Huang,[8] the increase in the passive film thickness is explained by an increase in the molybdenum content. The passivation mechanism and the processes

*Corresponding author; e-mail: kozuh@simet.hr

occurring in the passive region of the polarization curve are not fully understood. Electrochemical studies allow concluding that two types of passive film are formed on a Fe-24Cr alloy: a monolayer whose formation and reduction are reversible, and a multilayer film that actually forms the oxide film.[9] The chemical composition of the passive film formed on stainless steel in aqueous chloride solution varies with both the alloy composition, and the pH of the solution. Understanding and controlling passivity is the key factor for protecting stainless steel against pitting corrosion.

The ageing reactions and precipitation kinetics following exposure to high temperatures were much discussed research topics in the past. Mudali and Dayal[10] suggested that decomposition of delta ferrite and formation of sigma phase at the austenite/delta ferrite interfaces have a strong influence on pitting corrosion. Also, in a study by Park *et al.*[11] dealing with the influence of ageing on the corrosion resistance of ferritic stainless steel, E_{pit} values are reported to have diminished following increase in the sigma phase content. Similar behaviour has been observed for duplex steel.[12] In the literature, it has also been proposed that during the anodic dissolution of stainless steel materials the alloying elements chromium, molybdenum and nickel are enriched at the metal closest to the metal/passive film interface and nickel decrease the passive current, hence enhancing the passivation of the alloy.[13] Passive films are generally very thin. Those formed on stainless steels normally have a thickness of around δ = 5 nm.

A major disadvantage of austenitic stainless steels after PWHT is pitting corrosion, which occurs when they are exposed to chloride solutions. Cyclic polarization and electrochemical impedance spectroscopy are the methods most commonly used for studying pitting corrosion and determining the properties of passive oxide films.[13–15] As a non-destructive method for the evaluation of a wide range of materials, and one that makes use of a small amplitude AC signal, impedance spectroscopy has many advantages over other electrochemical techniques.[16,17]

A popular way to present the electrochemical impedance data is through the Nyquist plot. In this plot, the real impedance is plotted versus the imaginary impedance at each frequency used in the scan. This plot is helpful as the effects of capacitors, resistors and inductors are known at different frequencies. As the frequencies increase, the impedance of the capacitor decreases, the impedance of the resistor stays constant, and the impedance of the inductor increases. Knowing this, an equivalent circuit can be modelled from the data gathered.

According to the literature,[18] the formation and dissolution of the metal passive film comprise three steps: (a) penetration of metal atoms from the metal lattice to the passive film, (b) the ion mass transfer process in the passive film, and (c) the charge transfer process occurring at the passive film/solution interface. The total impedance (Z_T) of the interface between the passive metal electrode and the solution is:

$$Z_T = Z_{m/f} + Z_f + Z_{f/s} \quad (1)$$

The aim of this paper was to investigate, by cyclic polarization, electrochemical impedance spectroscopy and chronoamperometry, the effect of PWHT on the properties of passive films formed on AISI 316L austenitic stainless steel. To examine relative susceptibility to localized pitting corrosion, a w = 3.5 % NaCl solution was used. It is known that the corrosion properties of the weld metal are affected by the microstructural changes induced by PWHT. We attempted to establish a correlation between the sigma phase content that is known to produce a strong effect on the passive film properties, and resistance to pitting corrosion. Impedance measurements were performed to gain detailed information concerning contribution of the potential-dependent processes governing the passive current density. Various elements in the equivalent circuit were related to the metal/film and film/solution interfaces and to the characterization of the passive film.

Experimental

Commercial plates of AISI 316L stainless steel were welded using the manual electric arc welding method. The plate thickness was 15 mm. Before welding, the sheet surfaces were thoroughly cleaned and brushed. Welding of V-joints was carried out with the Böhler FOX SAS 4-A electrodes d = 2.5 and 3.25 mm in diameter. Table 1 shows the chemical compositions of the base and weld metals. Immediately after welding, the welded joint was subjected to PWHT at ϑ = 600–900 °C for two hours, and was then cooled in the air. The delta ferrite content of the weld metal was measured before PWHT and after it using a ferritoscope. The method

Table 1 – *Chemical composition of the base (BM) and weld metals (WM), w/%*

	C	Mn	Si	Cu	Mo	Cr	Ni	Nb
BM	0.026	1.49	0.45	0.35	2.04	16.75	10.80	0.016
WM	0.024	0.85	0.74	0.11	2.44	19.15	10.86	0.289

takes advantage of the fact that delta ferrite is magnetic and austenite is not.

After heat treatment, specimens were cut from the weld metal into smaller samples (d = 5 mm) for electrochemical measurements. The electrochemical behaviour was characterized by cyclic polarization and impedance spectroscopy.

Electrochemical measurements were performed with a conventional three-electrode cell using a platinum counter electrode, and the potentials were recorded at T = 293 K using an Ag/AgCl reference electrode. The working electrodes were prepared from AISI 316L weld metal before PWHT and after it. They were embedded in a Teflon holder having an exposed area of A = 0.2 cm^2. Measurements were carried out with a rotating-disc working electrode at the rotation rate of 1500 rpm. The samples were wet-ground to a 800 and 1200 grit finish, and then polished with Al_2O_3 slurry to obtain a mirror surface. Finally, the working electrode was ultrasonically cleaned (30 s) in ethanol and dried.

Experiments were carried out in a sodium chloride solution. The chloride medium (w = 3.5 % NaCl), pH 5.0, was prepared from analytical grade chemicals and distilled water. The solution was previously deaerated for 600 s with nitrogen to keep the system free of dissolved oxygen. Before measurement, the stabilization time of the working electrode at open circuit was t = 900 s.

Cyclic polarization, electrochemical impedance spectroscopy and chronoamperometry were performed by means of an "EG&G"-PAR Potentiostat/Galvanostat Model 263A with a Lock-in Amplifier Model 5210 operated under computer control. Cyclic polarization took place in the range of potentials from $E_{Ag/AgCl}$ = –1.0 V to +2.0 V, and from –1.0 V to +0.6 V, at the scan rate of v = 10 mV s^{-1}. Before each measurement the working electrode was cathodically polarized at $E_{Ag/AgCl}$ = –1.0 V for 300 s.

Impedance measurements were carried out using M398 software in the potential range from $E_{Ag/AgCl}$ = –1.0 V to +0.2 V. The working electrode was previously polarized at $E_{Ag/AgCl}$ = –1.0 V for 300 s. The frequency range was from f = 50 kHz to f = 40 mHz, and the amplitude of sinusoidal voltage U = 5 mV. The impedance data were numerically processed with ZsimpWin3.10 software (Princeton Applied Research, USA) employing Down-hill simplex method for optimatization. This method is basically a trial-and-error method. A function is evaluated at each assigned trial point and compared to each other. Based on the values at these points, the next trial points are determined. Function evaluations and comparison are repeated until a local minimum is reached. The goodness of overall fit is described by Chi-squared (χ^2) and the equivalent electrical circuits describing studied system were considered as acceptable when $\chi^2 < 10^{-3}$.

Chronoamperometric experiments were conducted in the potential range from $E_{Ag/AgCl}$ = –0.1 V to +0.1 V. The electrode was polarized at a selected potential and the current was monitored for 300 s. The working electrode was previously polarized at $E_{Ag/AgCl}$ = –1.0 V for 300 s.

Results and discussion

From polarization curves (I/E) it is possible to make predictions of the general corrosion behaviour of metallic surfaces in a chloride solution. Fig. 1 shows the cyclic, anodic and cathodic, polarization curves for 316L weld metal after PWHT (600–900 °C) in a w = 3.5 % NaCl solution (pH 5.0) at the v = 10 mV s^{-1} scan rate in the range of potentials $E_{Ag/AgCl}$ from –1.0 V to +2.0 V and from –1.0 V to +0.6 V. The electrochemical parameters obtained from the curves are listed in Table 2.

Table 2 – *Potentials and current calculated from cyclic polarization curves for the AISI 316L weld metal in w = 3.5 % NaCl solution before and after PWHT*

Temperature of PWHT, ϑ/°C	E_{corr}/V	I_{corr}/μA	E_{pit}/V	E_{rp}/V	E_{pass}/V	E_{pit}–E_{corr}/V
–	–0.264	6.39	0.586	0.032	–0.040	0.850
600	–0.566	8.75	0.497	–0.069	–0.205	1.063
700	–0.353	9.17	0.389	–0.020	–0.218	0.742
800	–0.421	0.98	0.324	–0.038	–0.223	0.745
900	–0.413	1.38	0.322	–0.028	–0.199	0.735

The scans exhibited comparable general features and were characterised by the appearance of a passive region and onset of pitting corrosion (Fig. 1). The active to passive transition was not observed. A relatively wide plateau of the potential-independent current indicated that passivity was present over a broad potential region, $E_{Ag/AgCl}$ from –1.0 V to +0.3 V (after PWHT). The absence of the active to passive transition on the I/E curves in Fig. 1 can be explained by the fact that even a brief contact of the working electrode with the moist air was sufficient to create a thin oxide layer on the electrode surface, which then prevented further active dissolution.

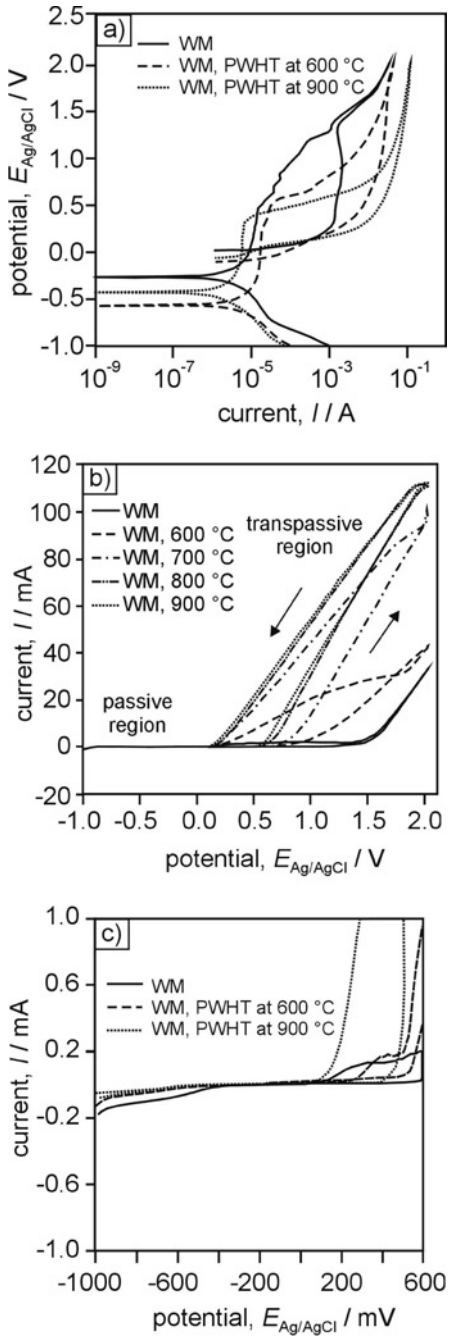

F i g . 1 – *Cyclic polarization curves of AISI 316L weld metal in w = 3.5 % NaCl solution in the potential range from $E_{Ag/AgCl}$ = –1.0 V to +2.0 V (a, b) and from $E_{Ag/AgCl}$ = –1.0 V to +0.6 V (c)*

Corrosion occurred as a result of anodic oxidation of iron:

$$Fe \rightarrow Fe^{2+} + 2\,e^- \qquad (2)$$

At the open-circuit potential, E_{corr} or V_{oc}, the current generated by the above reaction was balanced by the current generated by the cathodic reduction reaction of hydrogen evolution:

$$2\,H^+ + 2\,e^- \rightarrow H_2 \qquad (3)$$

The problem with austenitic stainless steel is not one of general corrosion but of pitting corrosion, which occurs in chloride media. Determination of the pitting potential is difficult because of unanticipated occurrence of pitting and unpredictable propagation rate. The current density increases with the increasing potential in the anodic direction owing to the transpassivation process preceding oxygen evolution. The current rises suddenly without any sign of oxygen evolution denoting a breakdown of the passive layer and nucleation of pitting corrosion. Fig. 2 shows the relationship between E_{pit} and PWHT temperature. It is interesting to note that the pitting corrosion of AISI 316L weld metal remarkably depends on the PWHT temperature. Higher E_{pit} values correspond to a stronger resistance to pitting corrosion. In general, as PWHT temperature increases there is a tendency for E_{pit} values to decrease.

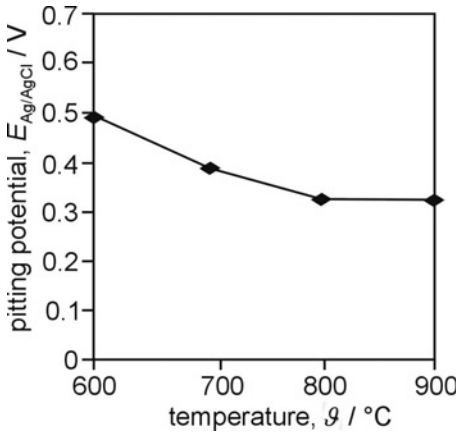

F i g . 2 – *Critical pitting potential as a function of PWHT temperature*

The corrosion resistance of alloys depends on not only the establishment of homogeneous passive films, but also on the individual material capability for repassivation. The results of cyclic polarization show insignificant E_{rp} changes as a result of increase in the PWHT temperature. From Table 2 is evident that $E_{rp} < E_{pit}$ and that pitting is not prevented. According to our results, PWHT had a negative effect on AISI 316L weld metal, because it decreased its resistance to pitting corrosion i.e. it reduced E_{pit} values (from 0.586 V to 0.322 V) and E_{pit}-E_{corr} values (from 0.850 V to 0.735 V) (Table 2).

This negative effect can be due to a change in microstructure, which takes place during PWHT. The microstructure, with its delta ferrite and austenite contents, and the partitioning of chemical constituents, plays an important role in explaining the corrosion behaviour. Before PWHT the microstructure of AISI 316L weld metal consisted

of w = 14.2 % delta ferrite. The delta ferrite fraction decreased with the increasing PWHT temperature (Table 3). According to our earlier investigations[19–21] delta ferrite is transformed into sigma phase by the reaction $\delta \rightarrow \sigma + \gamma_2$, where σ is sigma phase and γ_2 is secondary austenite. The sigma phase formation is concomitant with chromium and molybdenum depletion in ferrite which can trigger off pit nucleation and yield a ferrite phase more susceptible to corrosion. The ratio of delta ferrite decomposition into sigma phase increased from 17.6 % at 600 °C to 96.5 % at 900 °C. Indeed, the dependence of the pitting potential on microstructure is evident from Fig. 2.

Table 3 – *Delta ferrite content and decomposition ratio in AISI 316L weld metal after PWHT*

temperature of PWHT, ϑ/°C	600	700	800	900
δ-ferrite, w/%	11.7	8.0	0.9	0.5
decomposition ratio, %	17.6	43.6	93.7	96.5

The effect of PWHT on the corrosion resistance of AISI 316L weld metal in w = 3.5 % NaCl at T = 293 K was also assessed by electrochemical impedance spectroscopy. This is a well-established and powerful technique for testing *in situ* the phenomena that take place at a metal/solution interphase.

When the surface of austenitic stainless steel is immersed in chloride media, a passive film is naturally generated. Figs. 3–5 show the Nyquist and the Bode plots for the AISI 316L weld metal electrode immersed in a w = 3.5 % NaCl solution at different potentials. The chosen diagrams clearly portray a change in impedance with a change in the potential and PWHT temperature. The fitting parameters of the impedance plots are given in Tables 4–6. The simulated curves basically follow the experimental data from most measurements. The charge-transfer resistance values are strongly dependent on the passive film characteristics and are a measure of corrosion resistance.

Several equivalent circuits proposed in the literature to fit the experimental data for stainless steel were tested in this investigation.[18,22,23] The best results were obtained with the equivalent circuit shown in Fig. 6. Thereby, R_{el} is the ohmic resistance of the solution between the working and reference electrodes, Q is the constant phase element (CPE), W and L are the Warburg impedance and inductance at higher anodic polarization ($E_{Ag/AgCl}$ = +0.2 V). The CPE impedance (Z) has the form:

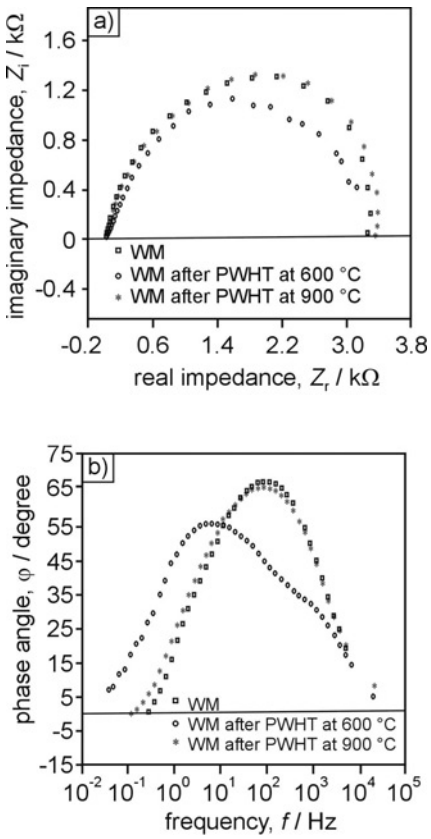

Fig. 3 – *Nyquist (a) and Bode (b) impedance diagrams of AISI 316L weld metal, in w = 3.5 % NaCl solution at $E_{Ag/AgCl}$ = –1.0 V, before and after PWHT*

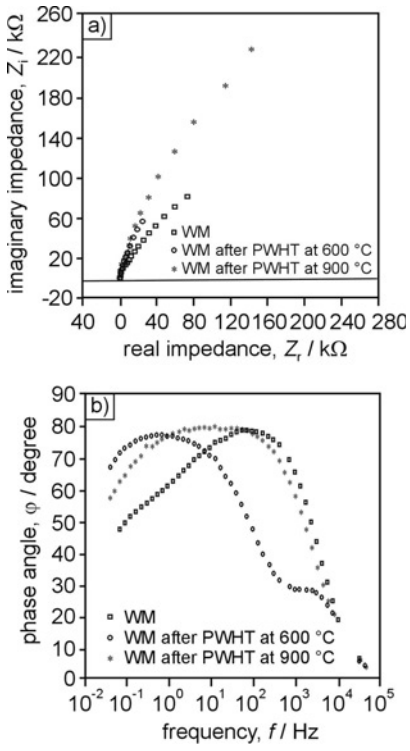

Fig. 4 – *Nyquist (a) and Bode (b) impedance diagrams of AISI 316L weld metal, in w = 3.5 % NaCl solution at $E_{Ag/AgCl}$ = +0.1 V, before and after PWHT*

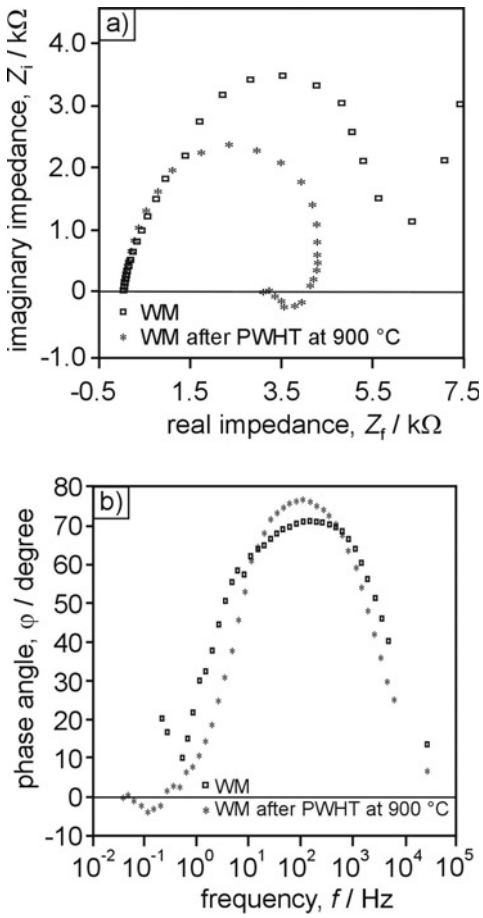

F i g . 5 – *Nyquist (a) and Bode (b) impedance diagrams of AISI 316L weld metal, in w = 3.5 % NaCl solution at $E_{Ag/AgCl}$ = +0.2 V, before and after PWHT*

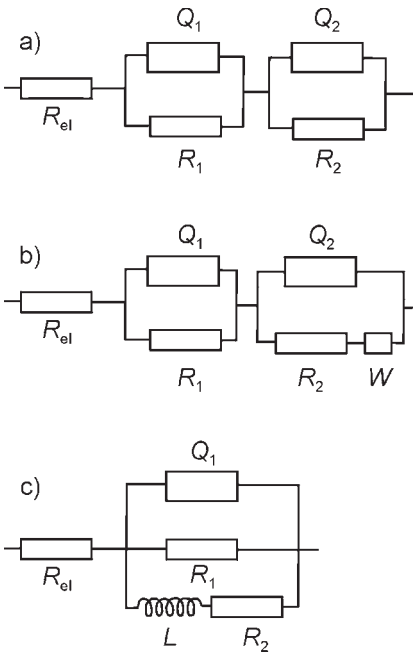

F i g . 6 – *Equivalent circuits used for fitting impedance data at different potential ranges: hydrogen evolution reaction and passive region (a), transpassive region (b, c)*

$$Z_{CPE} = [Q\ (j\ \omega)^n]^{-1} \quad (4)$$

where the coefficient Q is a combination of properties related to the surface and electroactive species, $j = \sqrt{-1}$, and ω is the angular speed (frequency) of the AC signal. The n value can be used as a gauge of heterogeneity of the electrode surface. Depending on n, CPE can represent resistance (n = 0, $Q = R$), Warburg impedance (n = 0.5, $Q = W$), or inductance (n = –1, $Q = L$).[24] Impedance measurements can be interpreted in terms of charge transfer resistance R_{ct}:

$$R_{ct} = \lim_{\omega \to 0} R(Z_f) \quad (5)$$

where $R(Z_f)$ denotes the real part of the complex faradaic impedance Z_f.

Oxide layer formed on the surface of stainless steel mostly has a duplex structure. The mechanism of passive film formation on stainless steel is governed by the thermodynamic stability of the oxidation products (oxides and hydroxides) at the appropriate pH and the potential. The inner layer is composed mainly of chromium oxides and has properties typical of p-type semiconductors, whereas the outer layer, formed by iron oxides and hydroxides, presents n-type semiconductor properties.[16] The results for the passive region obtained by the fitting procedure indicate that impedance measurements can detect such duplex structure. In this fashion, two RQ parallel circuits are used to represent the electrochemical activities of the passive film and the film/solution interface.[17] In Fig. 6, R_1 and Q_1 are the charge transfer resistance and capacitance at the AISI 316L weld metal/passive film interface i.e. the passive film layer having higher resistance values, and R_2 and Q_2 are the charge transfer resistance and capacitance relating to passive film/solution boundaries. It was assumed that total resistance R_T consisted of two parts, one proportional to the film thickness and another related to R_2. Quantitative analyses of the impedance data show that, as expected, the corrosion resistance was mainly afforded by the chromium-rich inner layer. In addition, the chi-squared values were $\chi^2 < 10^{-3}$ providing further evidence of good adjustment.

The impedance plot (Fig. 3) measured at $E_{Ag/AgCl}$ = –1.0 V showed a capacitive loop with relatively low R_T values. Those data were fitted to an equivalent circuit consisting of (R_1Q_1) and (R_2Q_2) series combinations. This behaviour was attributed to the hydrogen evolution reaction taking place at the passive surface. The hydrogen bubbles observed during impedance measurements disappeared by rotation of the working electrode at 1500 rpm. With a rise in the potential $E_{Ag/AgCl}$ from –1.0 V to +0.1 V the R_T values increased. Also, the R_T values grew higher with the increasing annealing temperature.

In the potential $E_{Ag/AgCl}$ region between –0.6 V and +0.1 V (i.e. passive region) the impedance plots were described with two (*RQ*) series. The Nyquist plot shown in Fig. 4 was characteristic of the full passive range.

At $E_{Ag/AgCl}$ = +0.2 V the appearance of a capacitive loop and the second time constant (Warburg impedance or inductance) could be noted (Fig. 5). At higher anodic potentials ($E_{Ag/AgCl} \geq$ +0.2 V), when the faradaic processes in the passive layer became more evident, the Warburg impedance and inductance *L* appeared. It is believed that the impedance of the passive films came from the migration of metal and oxygen vacancies within the film. Consequently, the impedance could be generated by diffusion phenomena. Inductance can be explained by dissolution of the passive film from the weld metal surface.[23]

Comparison of R_{pn1} values for different electrodes (Tables 4–6) shows that the values obtained for the weld metal before and after PWHT at ϑ = 600 °C were similar. After PWHT at ϑ = 900 °C R_{pn1} values were somewhat higher. The R_{pn2} values before and after PWHT at ϑ = 900 °C were similar, but they were much lower in the case of PWHT at 600 °C. It follows that the higher resistance of the weld metal after PWHT at 900 °C was the consequence of a thicker oxide layer. This is in accordance with the results in Table 2 where the lowest corrosion current was determined after PWHT at 900 °C. The corrosion current value for the weld metal after PWHT at 600 °C was slightly higher compared to that before PWHT. It follows that the corrosion resistance of the weld metal before PWHT at 600 °C and after it was inferior to that after PWHT at 900 °C. From Tables 4–6 it is also noticeable that Q_1 and Q_2 values were higher for the weld metal after PWHT at 600 °C than those before and after PWHT at 900 °C. This could be a consequence of a less compact passive film which increased the active area and thus raised the Q_1 and Q_2 values i.e. the capacitance values at the interfaces or within the layer. Lower *n* values could also account for increase in *Q* values.

Fig. 7 shows the chronoamperometric curves of AISI 316L weld metal after PWHT (ϑ = 600 and 900 °C) at different potentials of passive film formation. The current that flows through the passive film is:

$$i = i_0 \exp\left(\frac{\beta z F}{R T} \alpha \frac{\Delta \Phi}{\delta}\right) \qquad (6)$$

where i_0 is the exchange current, β is the transfer coefficient, *z* is the charge on the migrating species in the film, *F* is the Faraday constant, *R* is the universal gas constant, *T* is the temperature, *a* is the half-jump distance, $\Delta\Phi$ is the potential difference across the passive film and δ is the film thickness.

Table 4 – *Quantities of equivalent circuits for impedance measurement of AISI 316L weld metal in w = 3.5 % NaCl solution at different polarization potentials*

$E_{Ag/AgCl}$/V	Equivalent circuit	R_{el}/Ω	$Q_1 \cdot 10^5$/ $\Omega^{-1}s^n cm^{-2}$	n_1	R_{pn1}/ kΩ cm^2	$Q_2 \cdot 10^5$/ $\Omega^{-1}s^n cm^{-2}$	n_2	R_{pn2}/ kΩ cm^2	R_T/ kΩ cm^2
–1.0	R(QR)(QR)	18.33	14.81	1.0	0.407	14.69	0.83	0.221	0.628
–0.6	R(QR)(QR)	16.95	13.17	0.84	0.647	12.89	0.88	0.205	0.852
–0.5	R(QR)(QR)	18.12	9.09	0.97	0.971	32.01	0.75	0.250	1.221
–0.4	R(QR)(QR)	15.92	18.29	0.88	5.730	23.45	0.87	0.486	6.216
–0.3	R(QR)(QR)	16.78	17.73	0.90	9.796	15.50	0.88	1.921	11.717
–0.2	R(QR)(QR)	17.00	14.98	0.89	39.100	16.56	0.87	2.522	41.622
–0.1	R(QR)(QR)	16.95	18.56	0.83	50.600	12.96	0.87	3.400	54.000
0.0	R(QR)(QR)	16.51	8.29	0.93	93.760	12.21	0.91	3.580	97.340
0.1	R(QR)(QR)	17.26	7.67	0.91	33.900	6.86	0.90	2.338	36.238
0.2	R(Q(RW))(QR)	12.27	4.96	1.0	0.967	5.46	0.85	0.182	1.149

$W = 16.8 \cdot 10^{-5}$ $\Omega^{-1}s^{0.5}cm^{-2}$

$\chi^2 = 10^{-3}$–10^{-4}

Table 5 – *Quantities of equivalent circuits for impedance measurement of AISI 316L weld metal in w = 3.5 % NaCl solution at different potentials polarization, after PWHT at 600 °C*

$E_{Ag/AgCl}$/V	Equivalent circuit	R_{el}/Ω	$Q_1 \cdot 10^5$/ $\Omega^{-1}s^n cm^{-2}$	n_1	R_{pn1}/ kΩ cm^2	$Q^2 \cdot 10^5$/ $\Omega^{-1}s^n cm^{-2}$	n_2	R_{pn2}/ kΩ cm^2	R_T/ kΩ cm^2
–1.0	R(QR)(QR)	16.64	72.30	0.75	0.659	54.70	0.75	0.005	0.664
–0.6	R(QR)(QR)	15.27	71.05	0.81	1.634	118.25	0.65	0.006	1.640
–0.5	R(QR)(QR)	15.86	39.90	0.83	1.663	183.80	0.60	0.006	1.669
–0.4	R(QR)(QR)	16.86	56.20	0.85	6.560	77.1	0.70	0.014	6.574
–0.3	R(QR)(QR)	16.20	52.10	0.86	7.344	61.55	0.71	0.009	7.353
–0.2	R(QR)(QR)	22.62	37.95	0.88	46.16	55.55	0.80	0.010	46.170
–0.1	R(QR)(QR)	16.69	44.92	0.88	50.00	47.85	0.75	0.008	50.008
0.0	R(QR)(QR)	15.93	38.05	0.88	52.060	32.05	0.74	0.007	52.067
0.1	R(QR)(QR)	16.16	31.75	0.87	55.680	17.30	0.77	0.007	55.687
0.2	R(Q(RW))(QR)	16.64	2.39	0.86	2.122	12.79	0.80	1.808	3.930
						$W = 2.37 \cdot 10^{-2}$ $\Omega^{-1}s^{0.5}cm^{-2}$			

$\chi^2 = 10^{-3} - 10^{-4}$

Table 6 – *Quantities of equivalent circuits for impedance measurement of AISI 316L weld metal in w = 3.5 % NaCl solution at different potentials polarization, after PWHT at 900 °C*

$E_{Ag/AgCl}$/V	Equivalent circuit	R_{el}/Ω	$Q_1 \cdot 10^5$/ $\Omega^{-1}s^n cm^{-2}$	n_1	R_{pn1}/ kΩ cm^2	$Q_2 \cdot 10^5$/ $\Omega^{-1}s^n cm^{-2}$	n_2	R_{pn2}/ kΩ cm^2	R_T/ kΩ cm^2
–1.0	R(QR)(QR)	16.72	14.84	1.00	0.385	18.58	0.81	0.288	0.673
–0.6	R(QR)(QR)	16.62	11.61	0.86	0.460	81.80	0.79	0.338	0.776
–0.5	R(QR)(QR)	16.70	14.41	0.96	0.874	32.18	0.76	0.294	1.168
–0.4	R(QR)(QR)	15.56	14.40	0.91	5.838	60.80	0.74	0.769	6.607
–0.3	R(QR)(QR)	15.33	12.62	0.87	10.034	122.95	0.79	0.479	10.513
–0.2	R(QR)(QR)	16.20	11.85	0.87	60.800	175.35	0.71	0.540	61.340
–0.1	R(QR)(QR)	16.38	9.59	0.87	78.200	267.70	0.64	0.282	78.482
0.0	R(QR)(QR)	16.42	10.05	0.97	89.520	20.56	0.83	5.888	95.408
0.1	R(QR)(QR)	16.39	7.31	1.00	84.560	14.31	0.83	6.558	91.118
0.2	R(QR(LR))	16.17	3.63	0.92	0.948	$L = 8769$ H cm^2	–	3.008	3.988

$\chi^2 = 10^{-3} - 10^{-4}$

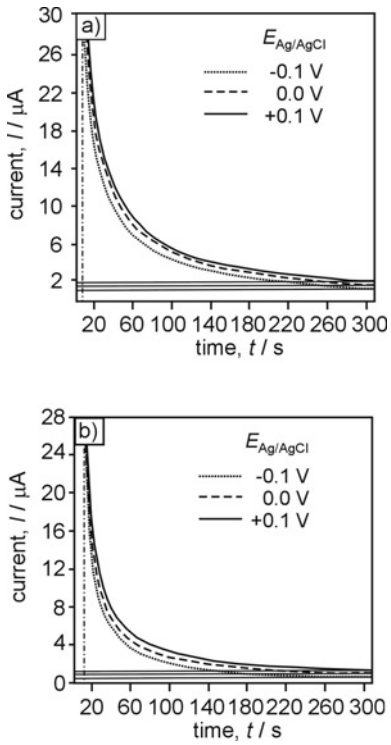

F i g . 7 – *Chronoamperometric curves of AISI 316L weld metal in w = 3.5 % NaCl solution at different potentials of passive film formation; a) after PWHT at 600 °C, b) after PWHT at 900 °C*

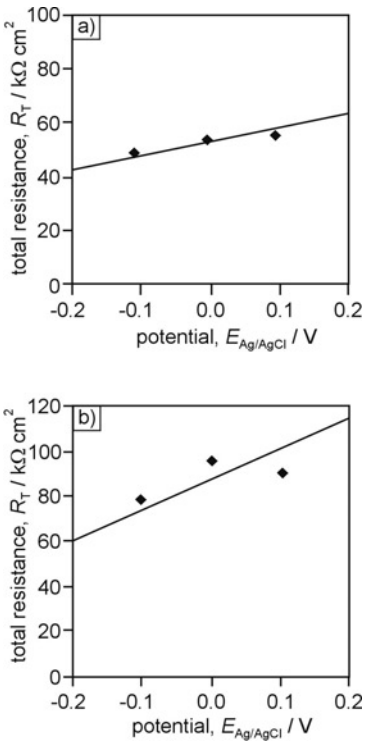

F i g . 8 – *Effect of the polarization potential in the full passive range on the total resistance of AISI 316L weld metal in w = 3.5 % NaCl solution; a) after PWHT at 600 °C, b) after PWHT at 900 °C*

Also, eq. (6) can be written as:

$$\delta = \frac{\beta z F}{R T} \alpha i R_{ct} = k' i R_{ct} \qquad (7)$$

R_{ct} is the resistance caused by charge transport in the passive film, $R_{ct} = R_T - R_{T,0}$ i.e. the difference between the R_T passivated at any potential in the full passive range and the R_T extrapolated to $E_{i=const.}$ (Fig. 8).

If $a = 0.5$ and $\beta = 0.5$ the calculated value of the coefficient $k`$ is 19.8 nm V^{-1} at 293 K.[17] All parameters for the calculated passive film thickness are given in Table 7. Thereby, the i current values in Table 7 were determined on the basis of the chronoamperometric curves at 300 s (Fig. 7). The thickness of the passive film calculated in this work ranged from δ = 1.1 to 5.3 nm. The higher thickness produced by PWHT at ϑ = 900 °C could be due to a heat input higher than after PWHT at ϑ = 600 °C. High heat input was likely responsible for easy oxidation of chromium into Cr_2O_3 during electrochemical measurements in w = 3.5 % NaCl.

T a b l e 7 – *Quantities for calculating the thickness of the passive film of AISI 316L weld metal after PWHT*

Temperature of PWHT, ϑ/°C	$E_{Ag/AgCl}$/ V	R_T/ kΩ cm^2	R_{ct}/ kΩ cm^2	i/ μA	$i\ R_{ct}$/ mV	δ/ nm
600	–0.1	50.008	8.008	1.390	55.66	1.1
	0.0	52.067	10.067	1.493	75.15	1.5
	0.1	55.687	13.687	1.746	119.49	2.4
900	-0.1	78.482	18.482	0.940	86.87	1.7
	0.0	95.408	35.408	1.516	268.39	5.3
	0.1	91.118	31.118	1.691	263.10	5.2

Conclusions

The passivation behaviour of AISI 316L weld metal before PWHT at ϑ = 600–900 °C and after it, in a w = 3.5 % NaCl solution of pH 5.0, was investigated by cyclic polarization, electrochemical impedance spectroscopy and chronoamperometry. The results suggest the following conclusions:

– The passivity of the weld metal was observed over a broad $E_{Ag/AgCl}$ potential region, from –1.0 V to +0.3 V. The pitting potential was higher before PWHT than after it.

– The effect of PWHT was negative as it decreased the resistance to pitting corrosion of the weld metal i.e. reduced E_{pit} values (from 0.586 V to 0.322 V) and $E_{pit} - E_{corr}$ values (from 0.850 V to 0.735 V).

– The pitting corrosion resistance of the weld metal in a chloride solution greatly deteriorated because of the nucleation and growth of sigma phase. This was likely due to chromium and molybdenum depletion in the areas adjacent to the sigma phase rich in those elements.

– The proposed equivalent electrical circuits allowed a good fit to the impedance data obtained.

– Impedance measurements showed the appearance of a hydrogen evaluation reaction in the cathodic region at $E_{Ag/AgCl}$ = –1.0 V.

– In the $E_{Ag/AgCl}$ potential range from –0.1 V to +0.1 V R_T values increased with the growing potential and the rising annealing temperature suggesting enhanced passive film thickness. Further increase in the potential ($E_{Ag/AgCl} \geq$ +0.2 V) led to activation of the working electrode and change of film thickness.

– The presence of Warburg impedance and inductance at $E_{Ag/AgCl}$ = +0.2 V suggested the diffusion of ions in/through the porous oxide passive film as well as its dissolution from the weld metal surface.

– The thickness of the passive film, calculated on the basis of electrochemical measurements was in the range from δ = 1.1 nm to 5.3 nm.

List of symbols and abbreviations

A – surface area, cm^2
d – diameter, mm
$E_{Ag/AgCl}$ – polarization potential, V
E_{corr} – corrosion potential, V
E_{pass} – passivation potential, V
E_{pit} – pitting potential, V
E_{rp} – repassivation potential, V
f – frequency, Hz
I_{corr} – corrosion current, A
i – current that flows through the passive film, A
k' – coefficient, nm V^{-1}
L – inductance, H cm^2
n – gauge of heterogeneity of the electrode surface
n_1 – gauge of the surface heterogeneity at weld metal/passive film interface
n_2 – gauge of the surface heterogeneity at passive film/solution boundaries
Q_1, Q_2 – capacitance, $\Omega^{-1}s^n cm^{-2}$
R_1, R_2 – ohmic resistance, Ω cm^2
R_{ct} – charge transfer resistance, Ω cm^2
R_{el} – ohmic resistance of the solution, Ω
R_{pn1} – charge transfer resistance at weld metal/passive film interface, Ω cm^2
R_{pn2} – charge transfer resistance at passive film/solution boundaries, Ω cm^2
R_T – total resistance, Ω cm^2
t – time, s
W – Warburg impedance, $\Omega^{-1}s^{0.5}cm^{-2}$
w – mass fraction, %
Z – impedance, kΩ
Z_i – imaginary impedance, kΩ
Z_r – real impedance, kΩ
δ – film thickness, nm
χ^2 – sum of the squares of the residuals
ϑ – temperature, °C
φ – phase angle, °
v – potential scan rate, mV s^{-1}
BM – base metal
CPE – constant phase element
PWHT – post-weld heat treatment
WM – weld metal

References

1. *Padilha*, *A. F.*, *Rios*, *P. R.*, ISIJ International **42** (4) (2002) 325.
2. *Sourmail*, *T.*, Materials Science and Technology **17** (1) (2001) 1.
3. *Lippold*, *J. C.*, *Kotecki*, *D. J.*, Welding Metallurgy and Weldability of Stainless Steels, John Wiley&Sons, Hoboken, New Jersey, 2005.
4. *Gooch*, *T. G.*, Welding Research **75** (5) (1996) 135s.
5. *Ševčiková*, *J.*, *Tuleja*, *S.*, *Kocich*, *J.*, "Corrosion Resistance of Stainless Steel Welds", Proc. of the Int. Welding Conference Welding Science&Technology, ed. Ivan Hrivňák, Faculty of Metallurgy Technical University of Košice, pp. 279–282, Košice, 1996.
6. *Hashimoto*, *K.*, *Asami*, *K.*, *Kawashima*, *A.*, *Habazaki*, *H.*, *Akiyama*, *E.*, Corrosion Science **49** (1) (2007) 42.
7. *Lula*, *R. A.*, Stainless Steel, American Society for Metals, Metals Park, Ohio, 1986.
8. *Huang*, *C. C.*, Corrosion Science **37** (5) (1995) 769.
9. *Dobbelaav*, *J. A. L.*, *Herman*, *E. C. M.*, *de Wit*, *J. H. W.*, Corrosion Science **33** (5) (1992) 765.
10. *Mudali*, *U. K.*, *Dayal*, *R. K.*, Materials Science and Technology **16** (4) (2000) 393.

11. *Park*, *C. J.*, *Ahn*, *M. K.*, *Kwon*, *H. S.*, Materials Science and Engineering **A 418** (1/2) (2006) 211.
12. *Bastos*, *I. N.*, *Tavares*, *S. S. M.*, *Dalard*, *F.*, *Nogueira*, *R. P.*, Scripta Materialia **57** (10) (2007) 913.
13. *Bastidas*, *J. M.*, *Torres*, *C. L.*, *Cano*, *E.*, *Polo*, *J. L.*, Corrosion Science **44** (3) (2002) 625.
14. *Polo*, *J. L.*, *Cano*, *E.*, *Bastidas*, *J. M.*, Journal of Electroanalytical Chemistry **537** (1/2) (2002) 183.
15. *Pardo*, *A.*, *Merino*, *M. C.*, *Carboneras*, *M.*, *Coy*, *A. E.*, *Arrabal*, *R.*, Corrosion Science **49** (2) (2007) 510.
16. *Kocijan*, *A.*, *Donik*, *Č.*, *Jenko*, *M.*, Corrosion Science **49** (5) (2007) 2083.
17. *Gojić*, *M.*, *Marijan*, *D.*, *Kosec*, *L.*, Corrosion **56** (8) (2000) 839.
18. *Ge*, *H. H.*, *Zhou*, *G. D.*, *Wu*, *W. Q.*, Applied Surface Science **211** (1–4) (2003) 321.
19. *Gojić*, *M.*, *Kožuh*, *S.*, *Kosec*, *L.*, *Tehovnik*, *F.*, Acta Metallurgica Slovaca **13** (13) (2007) 318.
20. *Kožuh*, *S.*, *Gojić*, *M.*, *Tehovnik*, *F.*, Microstructure of Welded Austenitic Stainless Steel AISI 316L After Post-Weld Heat Treatment, Proc. of the 12. Conf. on Materials, Processes, Friction and Wear, MATRIB`07, ed. Krešimir Grilec, HDMT, pp. 305–312, Vela Luka – Korčula, 2007.
21. *Gojić*, *M.*, *Kožuh*, *S.*, *Kosec*, *B.*, The Effect of Post-Weld Heat Treatment on Microstructure of AISI 316L Steel, Proc. of the IIW Int. Conf. Welding&Materials, Technical, Economic, and Ecological Aspects, HDTZ, pp. 765–773, Dubrovnik-Cavtat, 2007.
22. *Ningshen*, *S.*, *Mudali*, *U. K.*, *Amarendra*, *G.*, *Gopalan*, *P.*, *Dayal*, *R. K.*, *Khatak*, *H. S.*, Corrosion Science **48** (5) (2006) 1106.
23. *Macdonald*, *J. R.*, Impedance Spectroscopy, Emphasizing Solid Materials and Systems, John Wiley&Sons, New York, 1987.
24. *Bartos*, *B.*, *Hackerman*, *N.*, Journal of the Electrochemical Society **139** (12) (1992) 3428.